Astron. Astrophys. 325, 135–143 (1997)

ASTRONOMY AND ASTROPHYSICS

The distribution of stars and dust in spiral galaxies: the edge-on spiral UGC 2048

E.M. Xilouris[1,3], **N.D. Kylafis**[2,3], **J. Papamastorakis**[2,3], **E.V. Paleologou**[3], **and G. Haerendel**[4]

[1] University of Athens, Department of Physics, Section of Astrophysics, Astronomy & Mechanics, GR-15783 Athens, Greece
[2] University of Crete, Physics Department, P.O. Box 2208, GR-71003 Heraklion, Crete, Greece
[3] Foundation for Research and Technology-Hellas, P.O. Box 1527, GR-71110 Heraklion, Crete, Greece
[4] Max-Planck-Institut für Extraterrestrische Physik, D-85740 Garching b. München, Germany

Received 16 December 1996 / Accepted 18 March 1997

Abstract. We compare B, V, I surface photometry of the edge-on spiral galaxy UGC 2048 with corresponding surface photometry calculated from a realistic model of spiral galaxies, taking into account both absorption and scattering by dust. Our goal is to determine the distribution of stars and dust in the galaxy from the observed surface photometry. In the model that we use we assume that the stars and the dust in the disk are distributed axisymmetrically and exponentially in both directions, the radial and the perpendicular to the plane of the disk. The de Vaucouleurs $R^{1/4}$ law and the modified Hubble profile are used to fit the central region of the galaxy and a comparison is made between the two. For UGC 2048 we have found a face-on central optical depth of less than one in all three bands. This means that, if the galaxy were seen face-on, it would be transparent in the optical region of the spectrum, despite the prominent dust lane seen in the edge-on picture. We have also determined the scalelengths and scaleheights of the stars and the dust in the disk, the bulge characteristics and the inclination angle of the galaxy.

Key words: galaxies: photometry – galaxies: spiral – galaxies: individual: UGC 2048 – galaxies: ISM – ISM: dust, extinction

1. Introduction

The amount and distribution of dust in spiral galaxies remains an unsolved problem. For its solution, two approaches appear to be promising. The large N approach and the small N one.

The large N approach involves the statistical study of a large number of galaxies. Most of these studies examine how particular photometric parameters (such as surface brightness, colour, diameter, etc.) depend on the inclination angle of the galactic disk. Examples of such studies are those of Holmberg (1958), Heidmann et al. (1972), Valentijn (1990; 1994), Choloniewski (1991), Cunow (1992), Han (1992), Huizinga & van Albada (1992), Giovanelli et al. (1994; 1995) and Xu & Buat (1995). Because N is large, this approach is extremely useful for general conclusions concerning the opacity of spiral galaxies. However, the relatively simple galaxy models used in statistical studies, as well as possible selection effects that may bias the data sample (see Davies et al. 1993), can sometimes lead to wrong results.

The small N approach involves detailed study of the nearby spiral galaxies, which are well resolved. For this kind of approach, direct measurements of opacity, mainly using pairs of galaxies (Keel 1983; Andredakis & van der Kruit 1992; White & Keel 1992) as well as detailed modelling of galaxies (Kylafis & Bahcall 1987; Phillipps et al. 1991; Bosma et al. 1992; Byun 1993; Emsellem 1995; Beckman et al. 1996) are the most common ways to attack the problem. With the detailed model treatment, one has the advantage of deriving the parameters that describe the distribution of stars and dust in an accurate way. We believe that the small N approach will help a lot our understanding of the dust distribution in some galaxies and therefore in the minimization of the errors in the statistical studies (see also Byun et al. 1994). Several attempts have been reported so far to model the radiative transfer in galaxies (Kylafis & Bahcall 1987; Bruzual et al. 1988; Disney et al. 1989; Witt et al. 1992; Di Bartolomeo et al. 1995; Xu & Buat 1995; Bianchi et al. 1996; Corradi et al. 1996).

We have initiated a program to study the distribution of dust in galaxies using the small N approach. We will start with edge-on galaxies and then proceed to study less inclined ones. Edge-on galaxies have several advantages for this kind of work. One is that, in this view of a galaxy, one can easily separate the three main components of the galaxy (i.e., the stellar disk, the dust and the bulge). Another is that a lot of the details of a galaxy that are evident when the galaxy is seen face-on (e.g., spiral arms), are smeared out to a large degree when the galaxy is seen edge-on. Thus, a simple model with relatively few parameters can be used for the distribution of stars and dust in the galaxy. A third advantage is that the dust is very prominently seen in the dust lane.

Send offprint requests to: xilouris@physics.uch.gr

The first galaxy of our study is UGC 2048 (NGC 973) and the method we use is that of Kylafis & Bahcall (1987).

In Sect. 2 we describe the observations, in Sect. 3 we give the data reduction procedure, in Sect. 4 we present the model that we have used, in Sect. 5 we fit the model to the real data and we calculate the total amount of dust in the galaxy and in Sect. 6 we draw our conclusions.

2. Observations

Observations were made on the nights of September 8 and 9, 1994 with the 1.3 m telescope at Skinakas Observatory in Crete. The telescope is an $f/7.7$ Ritchey-Cretien. A CCD camera with a Thomson chip of 1024×1024 pixels of size 19 μm each was used for the observations. This arrangement corresponds to 0.39 arcsec/pixel and a field of view of approximately $7' \times 7'$. Assuming a distance of 63 Mpc for UGC 2048 (Gourgoulhon et al. 1992), the pixel size corresponds to 0.12 kpc. The chip was run with a gain of 3.33 e^-/ADU and showed a readout noise of 5.6 e^-. Exposures were made through B, V, I broad band filters. The B and V passbands are comparable to those of Johnson's photometric system, while the I passband is comparable to that of Cousin's photometric system. The effective wavelength of the system (filter and camera) in each passband is 0.443μm, 0.564μm and 0.809μm for the B, V, I bands respectively. During each night, three Landolt standard fields were observed at different airmasses. Each field had four to six standard stars. In this way, zero point, atmospheric extinction coefficient and colour terms could be obtained for the specific nights. Twilight flatfield frames were also taken in order to correct for pixel to pixel variation. The total integration time was 120 min in B, 50 min in V and 20 min in I. The seeing was 1.2″ and 1.4″ respectively for the two nights.

3. Reduction

3.1. General image reduction

Standard methods were used to analyse the data. First, the bias subtraction was done using a 40 000 pixel overscan region in each image. Both overscan regions and bias images showed that the bias level was very stable during the observations.

In order to create a flatfield frame in each filter, several (three to five) twilight sky images were taken, all shifted with respect to each other in order to avoid bright stars falling on the same position on the chip. Flatfield frames of the same filter were then combined using the IRAF task FLATCOMBINE. The pixel to pixel variation within the flatfield frame was then found to be less than 1% in all filters.

3.2. Calibration

After bias subtraction and flatfield correction was applied, photometry was done to standard stars and instrumental magnitudes were obtained. For photometry we used the DAOGROW algorithm (Stetson 1990) embedded in IRAF. Photometric magnitudes were taken from Landolt (1992). A three term calibration equation was then fitted to the data. The transformation equations are:

$$b = B + b_o + b_1 X_b + b_2(B - V)$$
$$v = V + v_o + v_1 X_v + v_2(B - V)$$
$$i = I + i_o + i_1 X_i + i_2(V - I)$$

where b, v, i are the instrumental magnitudes of the stars, B, V, I the catalogue magnitudes, X_b, X_v, X_i the airmasses, b_o, v_o, i_o the zero points in each filter, b_1, v_1, i_1 the atmospheric extinction coefficients and b_2, v_2, i_2 the colour correction terms.

After the fit was done, residuals between catalogue magnitudes and computed magnitudes were found to be less than 0.04 mags in B, 0.03 mags in V and 0.03 mags in I. All coefficients have insignificant variations from one night to the next. Atmospheric extinction coefficients were 0.23 mags/airmass in B, 0.17 mags/airmass in V and 0.04 mags/airmass in I. Having derived the coefficients, the transformation equations were inverted so that the galaxy images could be flux calibrated.

3.3. Galaxy image reduction

In order to make the galaxy data ready for the model, several procedures have been done, using the ESO-MIDAS data reduction package.

First, the cosmic rays were removed and the sky level was calculated and subtracted. A difficulty in the sky calculation was a bright star in the SW edge of the field, that produced a gradient in the background level. To solve this problem, a background fitting routine using a two-dimensional polynomial (linear in both directions) was applied. An artificial image of the sky was then produced and subtracted from the original image.

As a next step we had to consider the calculation of the data noise. In order to do this, we have followed the procedure described by Newberry (1991). Thus, sky noise, photon noise as well as readout noise were calculated in each individual galaxy frame. Then, after calibrating the galaxy images via the standard stars, a final image was produced in each filter by adding the individual images. The noise was then calculated for the summed image by taking into account the propagation of error. Finally a noise and a signal-to-noise mask of the galaxy image in each filter were produced. The set of pixels whose values lie in the trust region of three sigma were then selected. In V and I, most of the galaxy, even the faintest part within the dust lane, was above the three sigma level. In the B band, we had to lower our threshold to two sigma in order to include a large fraction of the central region of the galaxy where the dust is dominant.

In order to compare the observed galaxy with the model, we had to rotate the galaxy image in such a way, so that the major axis of the disk is horizontal. To do this, we fitted ellipses to the isophotes of the galaxy and characteristics such as the center and the position angle of the galaxy were determined. After the orientation of one image, all other images were aligned to that reference image.

Another step which proved to be very useful was to fold the galaxy. The model which we are going to use (and will be dis-

cussed in the next section) is axisymmetric. A visual inspection of the galaxy itself shows a symmetry around the vertical axis through the center. This led us to "cut" the galaxy into two parts along the minor axis through the center and add them together. This was found to be time saving because the model fit was done using only half of the pixels that cover the galaxy image, without any loss of accuracy. Furthermore, the existing fluctuations in the galaxy image are smoothed out to a large degree.

The final step was to remove all foreground stars. This was done using the IRAF task IMEDIT. In the defined aperture, the pixel values were replaced by zero so that the fitting program could ignore this part of the galaxy.

4. Model

In our model we assume that the stellar distribution consists of two components, the disk and the bulge. For the light distribution in spiral disks, two laws seem to be generally accepted so far. The sech^{2}z law (van der Kruit & Searle 1981) and the exponential law (Freeman 1970; Wainscoat et al. 1989). Both of these laws provide a good representation of the vertical distribution of light in the galactic disks. For the radial distribution, an exponential law is used. In the present work, we use the exponential law in both the radial and vertical direction.

For the bulge several profiles have been introduced. The well known $R^{1/4}$ law (de Vaucouleurs 1953; Young 1976), the Hubble-Reynolds law (Reynolds 1913; Hubble 1930), the Hernquist law (Hernquist 1990) and the exponential law (Andredakis & Sanders 1994) are good representations of bulges. For our model both the $R^{1/4}$ law and the Hubble profile are used and a comparison is made. A good description of the luminosity densities is given by Christensen (1990) for the $R^{1/4}$ law and by Binney & Tremaine (1987) for the Hubble law.

The stellar emissivity is then described by

$$L(R,z) = L_s \exp\left(-\frac{R}{h_s} - \frac{|z|}{z_s}\right) + \begin{cases} L_b(1+B^2)^{-3/2} & \text{for the Hubble law} \\ L_b \exp(-7.67B^{1/4})B^{-7/8} & \text{for the } R^{1/4} \text{ law}, \end{cases} \quad (1)$$

where R and z are the cylindrical coordinates, L_s is the stellar emissivity at the center of the disk and h_s and z_s are the scalelength and scaleheight respectively of the stars in the disk. The second term in this equation gives the two different types of bulge luminosity density profiles, the first being the Hubble law and the second the $R^{1/4}$ law, with L_b a normalization constant and

$$B = \frac{\sqrt{R^2 + z^2(b/a)^2}}{R_e}, \quad (2)$$

where R_e is the effective radius of the bulge and a and b are the semi-major and semi-minor axis respectively of the bulge. Because the $R^{1/4}$ profile has an infinite luminosity density at the center, and in order to avoid computational problems, the luminosity density in a small sphere of radius 0.2 kpc around the center was given a constant value and equal to that at 0.2 kpc. To be consistent, this region was excluded when the fitting procedure was done.

For the extinction coefficient we also use a double exponential law, namely

$$\kappa_\lambda(R,z) = \kappa_\lambda \exp\left(-\frac{R}{h_d} - \frac{|z|}{z_d}\right), \quad (3)$$

where κ_λ is the extinction coefficient at wavelength λ at the center of the disk and h_d and z_d are the scalelength and scaleheight respectively of the dust.

If the above model galaxy is seen edge-on, and for the moment we ignore completely the effects of dust, the surface photometry due to the disk alone, after integration of the first term on the right hand side of Eq. (1), is

$$I_{\text{disk stars}}(R,z) = 2L_s R K_1(R/h_s)\exp(-|z|/z_s), \quad (4)$$

where $K_1(x)$ is the modified Bessel function of the second kind, first order (Abramowitz & Stegun 1965), with a central value of

$$I_s = I_{\text{disk stars}}(0,0) = 2L_s h_s. \quad (5)$$

The central value of the bulge surface brightness is

$$I_b = I_{\text{bulge}}(0,0) = 2L_b R_e, \quad (6)$$

for the modified Hubble profile and

$$I_b = I_{\text{bulge}}(0,0) = 5.12L_b R_e, \quad (7)$$

for the de Vaucouleurs $R^{1/4}$ profile (Christensen 1990).

The optical depth through the disk, in directions parallel to the plane of the disk is

$$\tau_\lambda(R,z) = 2\kappa_\lambda R K_1(R/h_d)\exp(-|z|/z_d). \quad (8)$$

Thus, the central optical depth of an edge-on galaxy is $\tau_\lambda(0,0) = 2\kappa_\lambda h_d \equiv \tau_\lambda^e$ and the central optical depth of the same galaxy seen face-on is $\tau_\lambda(0) = 2\kappa_\lambda z_d \equiv \tau_\lambda^f$.

The radiative transfer is done in the way described by Kylafis & Bahcall (1987). The intensity I reaching a pixel is thought of as the sum of $I_0 + I_1 + I_2 + \cdots$, where I_0 consists of the photons that suffered no scattering between their point of emission in the galaxy and the pixel, I_1 consists of the photons that suffered one scattering between their point of emission and the pixel, I_2 consists of the photons that suffered two scatterings between their point of emission and the pixel, and so on. The term I_1 is proportional to the albedo ω of the dust, the term I_2 is proportional to ω^2 and so on. Since $\omega < 1$ (say $\omega \approx 0.6$, see below), the contribution to the intensity I of the terms I_n, with $n \geq 2$, is generally small compared to $I_0 + I_1$. Thus, to save computer time, we compute I_0 and I_1 very accurately and approximate the sum $\sum_{n=2}^{\infty} I_n$ with $I_0\, x^2/(1-x)$, where $x = I_1/I_0 < 1$ (see Eq. 19 of Kylafis & Bahcall 1987). The error that this approximation introduces to the intensity I is typically less than 1%.

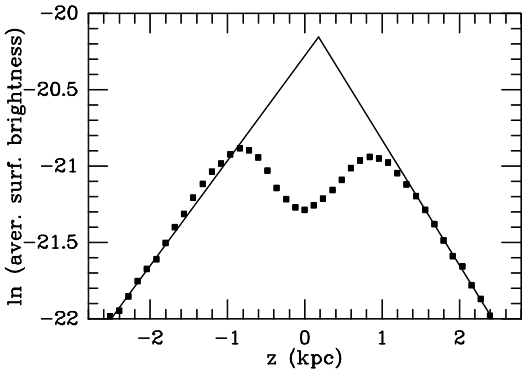

Fig. 1. Natural logarithm of the average surface brightness (squares) as a function of z for the parts of the galaxy away from the bulge. The solid lines give the slope of the average surface brightness at large z.

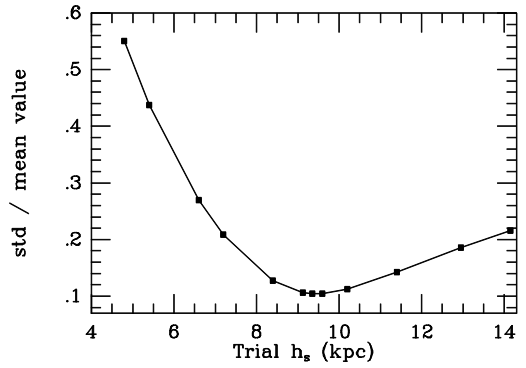

Fig. 2. Standard deviation over mean value versus trial h_s. The minimum corresponds to the best estimate for h_s.

For specific values of the parameters in Eqs. (1) - (3), a 2D image of a model galaxy is produced. The goal is to find those values of the parameters which create an image of the model galaxy as close as possible to the image of the observed galaxy. A Henyey-Greenstein phase function has been used for the scattering of the dust (Henyey & Greenstein 1941). A mean value 0.4 was used for the anisotropy parameter g, while the value 0.6 was used as an average albedo ω for all B, V, I bands. The effects of changing these parameters within the limits given by (Bruzual et. al. 1988) have been explored. It has been found that varying these parameters within the above limits has no important changes in the intensity because of the low optical thickness that has been found for this galaxy.

5. Model fitting

According to Eqs. (1) - (3), a fit to the surface photometry of a spiral galaxy should produce values of the parameters a) L_s (or equivalently I_s), z_s and h_s for the stars in the disk, b) L_b (or equivalently I_b), R_e and b/a for the stars in the bulge, c) κ_λ (or equivalently τ_λ^f), z_d and h_d for the dust and d) the inclination angle θ of the galactic disk with respect to our line of sight. The search for a minimum (in a least-squares sense) in a space of ten (the number of parameters) dimensions is not only time consuming but also contains the danger of ending up in a local minimum rather than the global one. For these reasons, it is helpful to get good estimates of as many parameters as possible before attempting a global fit of the galaxy.

5.1. Partial fitting

An inspection of the image of UGC 2048 reveals that this galaxy is seen approximately edge-on (the exact value of the inclination angle will be determined below). For an edge-on disk galaxy, the surface brightness away from the dust lane is proportional to $\exp(-|z|/z_s)$ at *all radial distances R* (see Eq. 4). Thus, excluding the central part of UGC 2048, which is affected by the bulge, the rest of the galaxy can be collapsed into one dimension parallel to the z axis. We do so in Fig. 1, where we have collapsed the galaxy between the radial distances 15 kpc and 25 kpc and the average value of the surface brightness in the I band as a function of z is shown. It is evident that for large $|z|$ the surface brightness falls exponentially with $|z|$, with a scaleheight z_s = 1.2 kpc (for the assumed distance, see end of Sect. 6.) derived from $z > 0$ and z_s = 1.4 kpc derived from $z < 0$. None of the two values is accurate (as we will see below), but they are good initial guesses for a global fit. The inaccuracy of z_s is due to both the bulge light and the exponential distribution of the dust. Between the two, the bulge light, which is present at faint levels even at large distances from the center, has a larger effect in the determination of z_s. For an estimate of the scalelength h_s of the stars in the disk, we collapse the galaxy perpendicular to the z axis. By avoiding the bulge and the dust lane, the rest of the galaxy should be well described by Eq. (4). Integrating this equation over z, we then ask for that value of h_s that will make the ratio

$$\frac{I_{\rm observ}}{RK_1(R/h_s)} \tag{9}$$

approximately constant at all R.

For each trial value of h_s we evaluate the ratio (9) for every R and compute the mean value and the standard deviation. Fig. 2 shows the ratio of the standard deviation to the mean value as a function of trial h_s. At the minimum we have the best estimate of the true h_s. At the assumed distance, this is 9.4 kpc in the I band. Again, this value is not accurate enough due to the contamination by the bulge and the dust. Having derived estimates for z_s and h_s, we use Eq. (4) to fit the surface brightness of the galaxy at a few positions away from the dust and the bulge. In this way, the central luminosity density L_s and thus the central surface brightness of the disk is estimated and has been found to be I_s = 18.7 mags/arcsec^2 in the I band.

Subtracting the derived image of the disk from the image of the galaxy, we are left with the image of the bulge away from the dust. From it we have found b/a = 0.45, I_b = 15 mags/arcsec^2 and R_e = 0.55 kpc for the Hubble profile, while I_b = 10 mags/arcsec^2 and R_e = 1.9 kpc for the $R^{1/4}$ profile in the I band.

Table 1. Global model fit parameters for UGC 2048. The Hubble profile is used for the bulge.

Parameter	Units	I band		V band		B band	
I_s	mags/arcsec^2	18.68	$\pm$0.05	19.81	$\pm$0.06	20.64	$\pm$0.05
z_s	kpc	1.01	$\pm$0.01	0.96	$\pm$0.02	0.89	$\pm$0.02
h_s	kpc	11.9	$\pm$0.2	12.4	$\pm$0.3	13.7	$\pm$0.1
I_b	mags/arcsec^2	15.55	$\pm$0.05	16.82	$\pm$0.08	17.48	$\pm$0.12
R_e	kpc	0.62	$\pm$0.02	0.58	$\pm$0.04	0.53	$\pm$0.06
b/a	–	0.45	$\pm$0.01	0.45	$\pm$0.01	0.44	$\pm$0.01
τ_λ^f	–	0.26	$\pm$0.01	0.48	$\pm$0.01	0.60	$\pm$0.01
z_d	kpc	0.50	$\pm$0.02	0.50	$\pm$0.01	0.54	$\pm$0.01
h_d	kpc	16.5	$\pm$0.3	16.1	$\pm$0.3	16.1	$\pm$0.4
θ	degrees	89.6	$\pm$0.1	89.6	$\pm$0.1	89.6	$\pm$0.1

Then, assuming that $h_d = h_s$, we fitted the analytic solution of the radiative transfer equation in the edge-on case (neglecting scattering) at a few points of the galaxy away from the bulge. From this we were able to determine z_d and τ_I^f, which were found to be 0.36 kpc and 0.25 respectively in the I band. Finally, using the numerical model, which is able to deal with any inclination angle, we fit the surface brightness at a few cuts of the galaxy parallel to the z axis by changing only the inclination angle. By trial and error, this parameter has been found to be approximately θ = 89.5 degrees. Again, these values are not accurate, but they are good initial guesses for the I-band data.

5.2. Global fitting

For the global fit we used the Levenberg-Marquardt algorithm (see Press et al. 1986) embedded in the IMSL MATH/LIBRARY. During this procedure, the radiative transfer is performed taking into account both absorption and scattering and a model galaxy is formed. Then, the observed surface brightness is compared with the computed surface brightness from the model and a new set of parameters is found. This is repeated until a minimum in the χ^2 value is reached. A 95% confidence interval on the regression parameters is also calculated, using the inverse of the Student's t distribution function.

Having at hand good initial guesses for the parameters, it was fairly easy to find the minimum. Tests were then made, with the initial values set more than 30% off the original values, in order to make sure that the minimum is indeed global. In all runs it was found that the final values derived from the fit were in the 95% confidence interval calculated.

The values of the parameters derived for UGC 2048 are shown in Table 1 for the case where the Hubble profile is used and in Table 2 for the $R^{1/4}$ law. All lengths are in kpc (see, however, our comment on the distance to the galaxy at the end of Sect. 6), while the central luminosity densities L_s for the stars in the disk and L_b for the stars in the bulge are given in terms of the central surface brightnesses I_s and I_b respectively (see Eqs. 5 - 7) in units of mags/arcsec^2. The optical depth $\tau_\lambda^f = 2\kappa_\lambda z_d$ is the central optical depth of the galaxy if it were to be seen face-on.

5.3. Dust content in the galaxy

Having derived the distribution of dust, it is straightforward to calculate the total amount of dust in the galaxy.

Assuming that the grains can be approximated by spheres of radius $a = 0.15\mu$m and material density $\rho = 3 \times 10^3$ kgr m^{-3}, the total mass of grain material is given by :

$$M_d = \frac{4\pi}{3}\frac{a^3\rho}{\sigma}\int \tau_V dS \tag{10}$$

where S is the surface area of the galaxy projected in the sky, τ_V is the optical depth in the V-band and σ is the extinction cross-section of a single grain and it is $\sigma \approx 1.5\pi a^2$ (see, e.g. Whittet 1992).

Using Eq. (8), which gives the optical depth through the disk in directions parallel to the plane of the disk and integrating over the whole projected surface of the galaxy, the dust mass is then given by :

$$M_d = 1.12 \times 10^6\ \tau_V^f\ h_d^2\ M_\odot \tag{11}$$

with h_d given in kpc.

Substituting the values of τ_V^f and h_d calculated from the model, the dust mass of the galaxy at the assumed distance of 63 Mpc is

$$M_d = 1.4 \times 10^8\ M_\odot \tag{12}$$

(see, however, our comment at the end of Sect. 6).

Using Eq. (2) of Devereux & Young (1990) and the published value for the H_I flux (Huchtmeier & Richter 1989) S_{H_I} = 8.83 Jy km s^{-1}, we calculated the atomic hydrogen mass, which was found to be

$$M(H_I) = 8.3 \times 10^9\ M_\odot \tag{13}$$

at the assumed distance. Unfortunately, we have not been able to locate a measurement for the 2.6 mm CO line for this galaxy in order to calculate the mass of molecular hydrogen $M(H_2)$. However, a crude approximation is to assume the same mass for molecular hydrogen as the mass we derived for atomic hydrogen (see, e.g. Table 1 in Devereux & Young 1990). If we do so, the total gas mass is approximately

$$M_g = 1.7 \times 10^{10}\ M_\odot. \tag{14}$$

Table 2. Global model fit parameters for UGC 2048. The $R^{1/4}$ law is used for the bulge.

Parameters	Units	I band		V band		B band	
I_s	mags/arcsec^2	18.43	$\pm$0.06	19.36	$\pm$0.06	20.50	$\pm$0.08
z_s	kpc	1.00	$\pm$0.02	0.93	$\pm$0.02	0.87	$\pm$0.02
h_s	kpc	11.0	$\pm$0.3	11.0	$\pm$0.12	11.3	$\pm$0.15
I_b	mags/arcsec^2	9.07	$\pm$0.11	9.62	$\pm$0.10	10.58	$\pm$0.11
R_e	kpc	2.38	$\pm$0.10	1.69	$\pm$0.08	1.67	$\pm$0.07
b/a	–	0.44	$\pm$0.01	0.45	$\pm$0.01	0.46	$\pm$0.01
τ_λ^f	–	0.30	$\pm$0.01	0.52	$\pm$0.01	0.65	$\pm$0.01
z_d	kpc	0.57	$\pm$0.01	0.59	$\pm$0.01	0.57	$\pm$0.01
h_d	kpc	16.5	$\pm$0.4	16.2	$\pm$0.5	16.1	$\pm$0.5
θ	degrees	89.6	$\pm$0.1	89.6	$\pm$0.1	89.6	$\pm$0.1

Finally, from the above calculations, the gas to dust ratio for this galaxy is found to be

$$\frac{M_g}{M_d} = 121 \tag{15}$$

which is close to the value of $\sim$ 100 that is widely adopted for our Galaxy (Spitzer 1978, p.162).

6. Conclusions

Through three dimensional axisymmetric modelling of the stars and the dust in UGC 2048, we have been able to determine the parameters that describe the distribution of stars and dust in this galaxy. Fig. 3 shows the 2D image of UGC 2048 in the I, V and B bands (top to bottom) with the model in the left half of the frame and the folded real galaxy in the right half of each panel. The model galaxy reproduces very well the real galaxy. We have verified this by taking the residuals between the observed galaxy and the model galaxy that we produced. Fig. 4 shows how the residuals in the I band are distributed throughout the galaxy's image, in terms of the absolute value of the percentage error. Different colours indicate areas with different error values. Red colour corresponds to areas with error less than 10%, yellow colour corresponds to areas with error between 10% and 20%, and black colour corresponds to areas with error between 20% and 30%. White circles indicate the positions of the foreground stars. In the upper panel, a de Vaucouleurs $R^{1/4}$ profile was used for the bulge, while a Hubble profile was used in the bottom panel. The distribution of residuals in the B and V bands is similar to the one in the I band.

Fig. 4 has a lot more information than discussed above. First of all it gives us an idea of the quality of the fit that was done to the observed image. For the $R^{1/4}$ law bulge (top panel), the red colour (error less than 10% in absolute value) covers 46% of the total image of the galaxy, while the red and the yellow colours (error less than 20%) cover 80% of the total image. Only 4% of the total image has errors grater than 30%. For the Hubble bulge (bottom panel), 43% of the total galaxy image has error less than 10%, while in 76% of the galaxy's image the error is less than 20%. In this case, 5% of the total image has errors grater than 30%. Considering the three-dimensional clumpiness and the spiral structure that the real galaxy may have, these numbers show on the one hand the goodness of the fit and on the other the validity of the 3D stellar and dust distributions of the model galaxy that we have used.

Another thing that these residual maps show us is a hint at the detailed structure and clumpiness of the real galaxy. The clumpiness in the 3D distribution of stars and dust is recognized by the regions of the galaxy where the observed surface brightness has a large difference from a smooth distribution. In other words, regions in the residual maps (between the observed galaxy and the smooth model) with high errors indicate that along the line of sight the 3D distribution of stars and dust has significant departures from the assumed smooth distribution. These departures could be due to spiral structure or just inhomogeneities. For example, one can see in Fig. 4 small black regions near the major axis of the galaxy that are caused probably by inhomogeneities, i.e., by local departures from the smooth 3D distribution. Similarly, relatively large black and yellow areas in the galactic disk away from the major axis may indicate the existence of spiral arms. Also, one can easily spot four "lobes" distributed symmetrically around the center of the galaxy in the bulge region. These features come from the fact that the projection of the bulge in the plane of the sky has a characteristic "box/peanut" shape and differs from the commonly used $R^{1/4}$ or Hubble profiles.

Yet another thing that comes from Fig. 4 is a direct comparison of the two types of bulge that we have used. It is evident that the bulge of the galaxy is described somewhat better with the $R^{1/4}$ law (top panel) than with the Hubble law (bottom panel) especially at the outer regions of the bulge.

We also want to stress from Fig. 4 the fact that the model stellar disk and the model dust distribution characteristics are not affected significantly by the different types of bulge that we have used. This is also evident from Tables 1 and 2, where the various derived parameters are shown. Apart from the different bulge characteristics, because two completely different functions are used, only small differences are seen for the parameters that describe the exponential distributions of the dust and the stars in the disk. This gives us the freedom to use any of these two types of bulges when the aim is to derive only stellar disk and dust distribution characteristics.

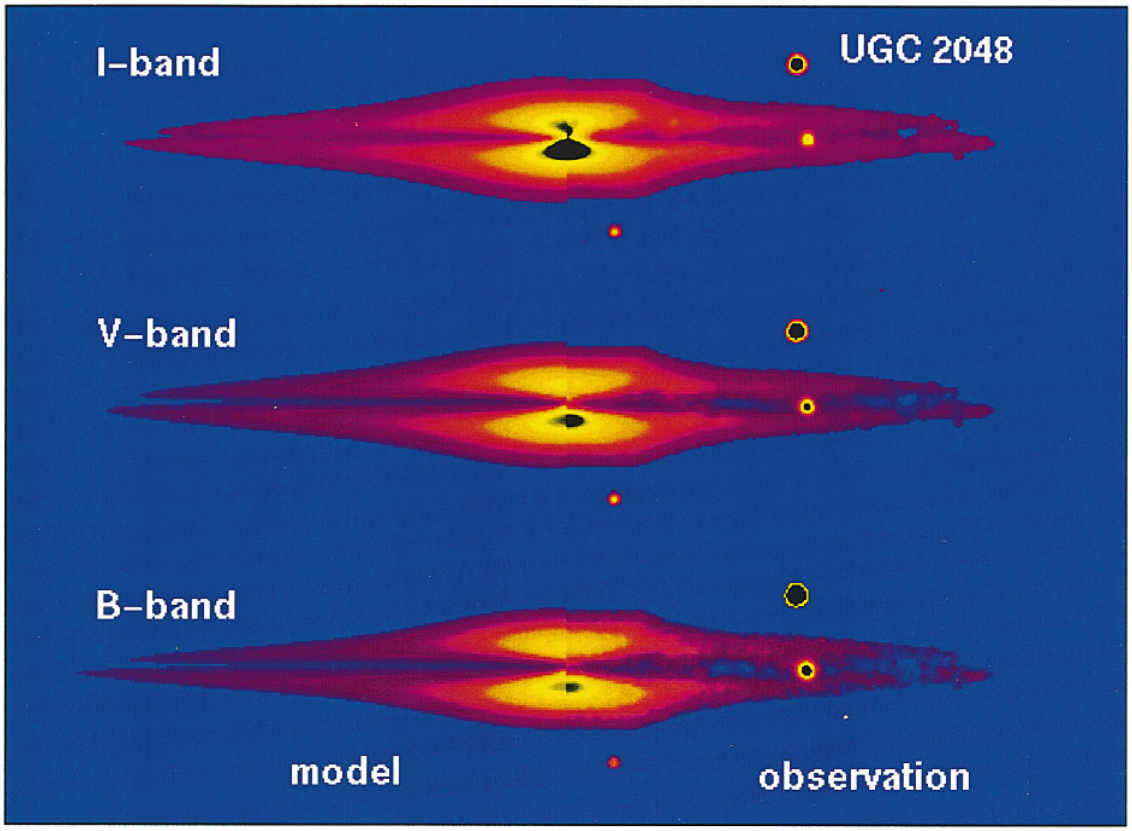

Fig. 3. Image of UGC 2048 in I band (top), V band (middle) and B band (bottom). The left half in each panel is the model image and the right half is the real galaxy image.

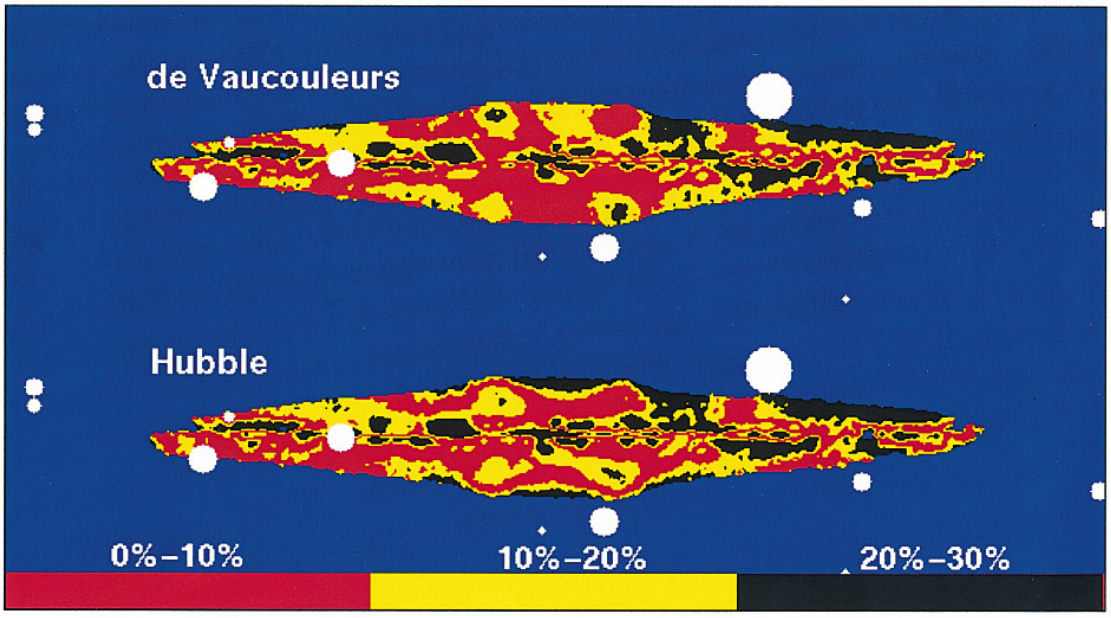

Fig. 4. Colour map, showing the relative error between the observed I band image and the model galaxy. See text for a detailed description.

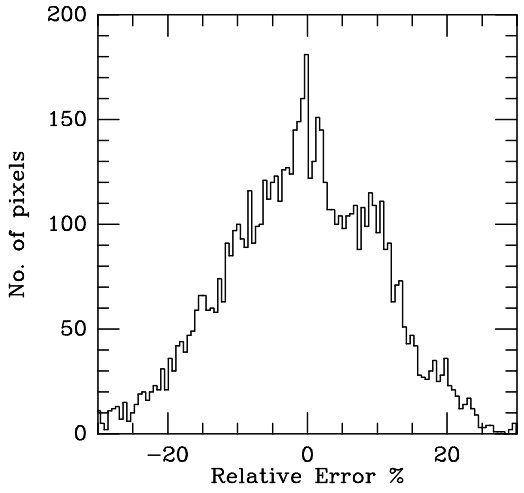

Fig. 5. Histogram of the relative errors between the real image and the model image of the galaxy

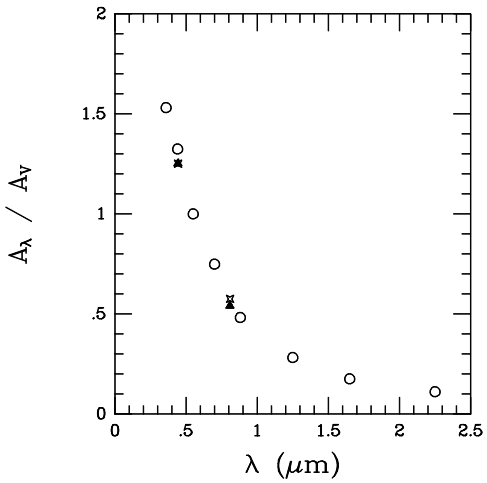

Fig. 6. The observed (open circles) values of A_λ/A_V for our Galaxy and the values calculated from the model (solid triangles for the Hubble case and stars for the $R^{1/4}$ case) for UGC 2048

One may claim that the structure and the inhomogeneities in the 3D distribution of stars and dust in the galaxy make it practically impossible to find smooth distributions to describe the galaxy. This would certainly be the case if one tried to fit only a small part of the galaxy. Fortunately, by doing a global fit and taking into account the whole image of the galaxy, the model tries to cancel out these inhomogeneites and a mean distribution of the light emissivity is evaluated. As a result, there are regions in the image of the galaxy where the residuals are positive and regions where they are negative, distributed in such a way as to accomplish the highest possible symmetry between positive and negative values. This is shown in Fig. 5, where a histogram of the percentage relative errors between the *folded* observed image (in which the fit was done) and the model image is shown for the case where the de Vaucouleurs bulge is used.

Once the distribution of light in the galaxy was determined, we wanted to investigate how dust behaves if for the moment we neglect scattering and assume that only absorption takes place. To do this we fitted the model image to the galaxy image again, but now only the optical depth of the dust was left as a free parameter. It was found that the central optical depth of the dust dropped by about 30% in all three bands. This indicates that scattering plays an important role in the determination of the galaxy characteristics and a serious underestimate of the opacity can be made if only absorption is considered. This conclusion was also reached by other authors (see, e.g. Bruzual et al. 1988, Di Bartolomeo et al. 1995, Corradi et al. 1996).

From the face-on central optical depth of the dust $\tau_\lambda^f = 2\kappa_\lambda z_d$, and given a mean value of the scaleheight z_d for all the filters, one can calculate the absorption coefficient κ_λ in each band. We have found that κ_B/κ_V = 1.250(1.250) and κ_I/κ_V = 0.541(0.576) for the case where the Hubble ($R^{1/4}$) law is used. These values can be directly compared with the ratio of the extinction A_λ/A_V and are plotted as a function of the effective wavelength in Fig. 6. Solid triangles (stars) correspond to the values derived with our model for the case where the Hubble ($R^{1/4}$) law is used. The open circles are the values given by Rieke & Lebofsky (1985) for our Galaxy.

Finally, we would like to point out that all the characteristic lengths of the stellar and dust distribution have been found to be larger by about a factor of two compared to mean values for these lengths derived for a number of galaxies (see, e.g. Byun 1992). Thus, we caution the reader that the reported distance of 63 Mpc might be an overestimate by a factor of 2 from the true distance. In this case, where the distance is half of that reported above, the dust and the gas masses become M_d = 3.5 × 10^7 $M_\odot$ and M_g = 4.25 × 10^9 $M_\odot$, leaving the gas to dust ratio unchanged and equal to 121.

Acknowledgements. We thank the referee (R. Corradi) for his useful comments and suggestions for improving the paper. We also thank P. Alton for his contribution in the calculation of the dust mass. One of us (E.M.X.) would like to thank T. Pierratos for useful discussions concerning analytical calculations for the bulge functions. This research has been supported in part by a Greek-British Joint Research Program and by a P.EN.E.D. Program of the General Secretariat of Research and Technology of Greece. Skinakas Observatory is a collaborative project of the University of Crete, the Foundation for Research and Technology-Hellas and the Max-Planck-Institut für Extraterrestrische Physik.

References

Abramowitz M., Stegun I.A., 1965, Handbook of Mathematical Functions. Dover, New York

Andredakis Y.C., van der Kruit P.C., 1992, A&A, 265, 396

Andredakis Y.C., Sanders R.H., 1994, MNRAS, 267, 283

Beckman J.E., Peletier R.F., Knapen J.H., Corradi R.L.M., Gentet L.J., 1996, ApJ, 467, 175

Bianchi S., Ferrara A., Giovanardi C., 1996, ApJ, 465, 127

Binney J., Tremaine S., 1987, Galactic Dynamics. Princeton Univ. Press, Princeton

Bosma A., Byun Y., Freeman K.C., Athanassoula E., 1992, ApJ, 400, L21
Bruzual G.A., Magris G.C., Calvet N., 1988, ApJ, 333, 673
Byun Y.I., 1992, Ph.D. thesis, Australian National University
Byun Y.I., 1993, PASP, 105, 993
Byun Y.I., Freeman K.C., Kylafis N.D., 1994, ApJ, 432, 114
Choloniewski J., 1991, MNRAS, 250, 486
Christensen J.H., 1990, MNRAS, 246, 535
Corradi R.L.M, Beckman J.E., Simonneau E., 1996, MNRAS, 282, 1005
Cunow B., 1992, MNRAS, 258, 251
Davies J.I., Phillipps S., Boyce P.J., Disney M.J., 1993, MNRAS, 260, 491
de Vaucouleurs G., 1953, MNRAS, 113, 134
Devereux N.A., Young J.S., 1990, ApJ, 359, 42
Di Bartolomeo A., Barbaro G., Perinotto M., 1995, MNRAS, 277, 1279
Disney M., Davies J., Phillipps S., 1989, MNRAS, 239, 939
Emsellem E., 1995, A&A, 303, 673
Freeman K.C., 1970, ApJ, 160, 811
Giovanelli R., Haynes M.P., Salzer J.J., et al., 1994, AJ, 107, 2036
Giovanelli R., Haynes M.P., Salzer J.J., et al., 1995, AJ, 110, 1059
Gourgoulhon E., Chamaraux P., Fouque P., 1992, A&A, 255, 69
Han M., 1992, ApJ, 391, 617
Heidmann J., Heidmann N., de Vaucouleurs G., 1972, Mem. R. Astron. Soc., 76, 121
Hernquist L., 1990, ApJ, 356, 359
Henyey L.G., Greenstein J.L., 1941, ApJ, 93, 70
Holmberg E., 1958, Medd. Lunds Obs., Ser. 2, No 136
Hubble E.P., 1930, ApJ, 71, 231
Huchtmeier W.K., Richter O.G., 1989, A general catalog of H_I observations of galaxies, New York, Springer-Verlag
Huizinga J.E., van Albada T.S., 1992, MNRAS, 254, 677
Keel W.C., 1983, AJ, 88, 1579
Kylafis N.D., Bahcall J.N., 1987, ApJ, 317, 637
Landolt A., 1992, AJ, 104, 340
Newberry M., 1991, PASP, 103, 122
Phillipps S., Evans Rh., Davies J.I., Disney M.J, 1991, MNRAS, 253, 496
Press W.H., Flannery B.P., Tenkolsky S.A., Vetterling W.T., 1986, Numerical Recipes. Cambridge Univ. Press, Cambridge
Reynolds J.H., 1913, MNRAS, 74, 132
Rieke G.H., Lebofsky M.J., 1985, ApJ, 288, 618
Spitzer L., 1978, Physical Processes in the Interstellar Medium, New York, Wiley-Interscience
Stetson P., 1990, PASP, 102, 932
Valentijn E.A., 1990, Nat, 346, 153
Valentijn E.A., 1994, MNRAS, 266, 614
van der Kruit P.C., Searle L., 1981, A&A, 95, 116
Wainscoat R.J., Freeman K.C., Hyland A.R., 1989, ApJ, 337, 163
White R.E, Keel W.C., 1992, Nat, 359, 129
Witt A.N., Thronson H.A., Capuano J.M., 1992, ApJ, 393, 611
Wittet D.C.B., 1992, Dust in the galactic enviroment, IOP publishing ltd.
Xu C., Buat V., 1995, A&A, 293, L65
Young P.J., 1976, AJ, 81, 807

This article was processed by the author using Springer-Verlag LaTeX A&A style file *L-AA* version 3.